ChemComm

Accepted Manuscript

ROYAL SOCIETY OF CHEMISTRY

rsc.li/chemcomm

ROYAL SOCIETY OF CHEMISTRY View Article Online
DOI: 10.1039/C9CC00764D

Journal Name

COMMUNICATION

Traceable Cancer Cell Photoablation with A New Mitochondria -Responsive and -Activatable Red-Emissive photosensitizer

Received 00th January 20xx,
Accepted 00th January 20xx

DOI: 10.1039/x0xx00000x

www.rsc.org/

Chenlin Yang,[a,c] Rui Hu,[*a] Fengxian Lu,[a,c] Xudong Guo,[a] Shuangqing Wang,[a] Yi Zeng,[*b,c] Yi Li [b,c] and Guoqiang Yang[*a,c]

A mitochondria-responsive and -activatable photosensitizer (PS), MPS, composed of pyridinium cation as mitochondria targeting group and dibenzylideneacetone derivative with environment-sensitive emission property as the ROS generator and self-efficacy tracer is reported. This multifunctional PS offers a new strategy for traceable photodynamic ablation of cancer cells.

The increasing emergence of drug resistance and side effects during cancer therapy urges developments of novel drugs or therapeutics for future treatments. Photodynamic therapy (PDT) is a minimally invasive treatment involving a photosensitizer (PS) as the drug in combination with light and oxygen. The therapy is initiated upon photoirradiation which gives rise to reactive oxygen species (ROS) after serial photochemical processes. ROS attack various biological species in cells resulting in apoptosis or necrosis of cells and consequent treatment of diseases.[1] The highly reactive ROS with relatively short lifetime and light dependence provide multiple-targets destruction within the irradiation-confined killing zone, which make PDT a promising treatment with little drug resistance and highly spatial selectivity.

PSs such as porphyrin derivatives have been approved for clinical applications for many diseases, including cancer treatments.[2-6] Currently, the development of PSs is entering the stage of smart drugs that are capable of cell or organelle targeting and imaging, aiming to increase therapeutic effects and lower down side effects at the same time.[7-10] Various targeting ligands, such as antibodies,[11] RGD peptide,[12-14] aptamers,[15, 16] 2-deoxyglucose,[17] and triphenylphosphonium,[10] have been attached to PSs to enhance drug delivery to diseased cells and organelles. Introducing activation step to PSs is another strategy to manipulate PSs and PDT, by which PSs become phototoxic only when they are activated or released by disease-related enzymes[18-21] or microenvironment in targets.[22-24] Furthermore, to minimalize side effects on normal cells, strategies by integrating indicators of PDT response into PSs have also attracted increasing attentions.[25] For example, the PSs with a built-in singlet oxygen sensor[26] have been developed to kill cancer cells and indicate $^1O_2$ generation simultaneously. Another smart design *via* combination of apoptosis-associated enzyme substrate[20,27]into PS was also achieved the direct reporting of therapeutic response. However, the challenging molecular design and synthetic routes are frustrating. Therefore, it is still appealing to develop simple and efficient strategies for traceable cancer therapy.

Mitochondria are indispensable cellular organelles responsible for the major energy supply for cells, and involved in many other cellular networks, including cell growth, differentiation and apoptosis.[28, 29] On account of the high susceptibility to reactive oxygen species (ROS) damage, mitochondria are idea targets for virous drugs and chemotherapies especially PDT treatment.[30-36] Herein, a red emissive dibenzylideneacetone derivative P1 with obviously

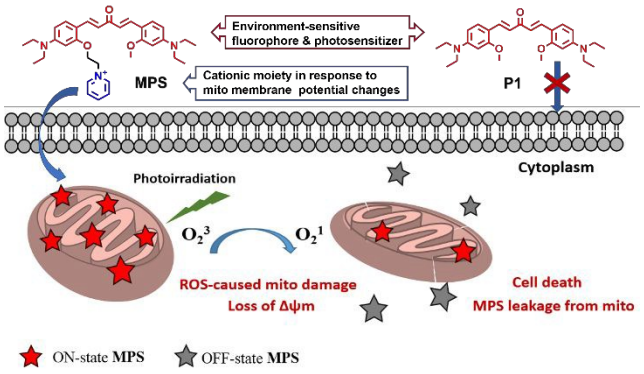

Scheme 1. Structure of MPS and schematic illustration of MPS used for cell photoablation and the resulting cytotoxicity report.

[a] *Beijing National Laboratory for Molecular Sciences (BNLMS), Key Laboratory of Photochemistry, Institute of Chemistry, Chinese Academy of Sciences, Beijing 100190, China*
[b] *Key Laboratory of Photochemical Conversion and Optoelectronic Materials, Technical Institute of Physics and Chemistry, Chinese Academy of Sciences, Beijing 100190, China*
[c] *University of Chinese Academy of Sciences, Beijing 100049, China*
Electronic Supplementary Information (ESI) available: [details of any supplementary information available should be included here]. See DOI: 10.1039/x0xx00000x

environment-sensitive emission property[37] was first built off. Owing to the enhanced spin-orbit coupling and intersystem crossing channel supported by the central electron-withdraw ketone in the molecular scaffold,[38] P1 presents conspicuous ROS generation and photosensitization functions. In order to endow this new scaffold with traceability, pyridinium cation, a reversible mitochondria-guiding ligand, was selected to be tethered then a new hydrophilic PS, MPS, with special affinity to mitochondrial components and sensitive response to mitochondrial membrane potential (MMP) changing, was obtained. The differences of MPS and P1 are illustrated in Scheme 1. MPS exhibits comparable environment -dependent emission and $^1O_2$ generation but much improved aqueous compatibility with P1. Different from the low staining efficiency of P1 nanoaggregates in cells, MPS guided with the pyridinium unit highly accumulates on active mitochondrial components where its red fluorescence is turned on because of the relatively lower polarity of inner mitochondrial membrane. Upon light irradiation, the bound MPS can be activated to generate $^1O_2$ efficiently which initiates MMP disruption and the following cell apoptosis. After that MPS is released from mitochondria to cytoplasm, where the environment polarity is increased and the fluorescence is switched off, showing self-reporting capability of apoptosis induced by ROS damage to mitochondria. Meanwhile, the generation of $^1O_2$ is also reduced, deterring the overproduction of oxidative species.

The fluorescence spectra of MPS and P1 in different solutions were firstly recorded and shown in Figure S1. Both MPS and P1 presented positive solvatochromism with remarkable emission shifts of about 100 nm as increasing the polarity of solvents, which demonstrated the typical intramolecular charge transfer (ICT) property of the used dibenzylideneacetone scaffold. The fluorescence quantum yield (ΦF) of P1 kept above 0.1 in all solvents even though it forms into aggregates in water. While the ΦF of MPS lowered to nearly one third of P1 in organic solvents because of the introduction of electrophilic pyridinium unit, and a more than 40-fold decrease of the emission intensity at 600 nm was detected in water compared to that in EtOH (in Figure 1A), indicating MPS can be used as a smart turn-off indicator for environment polarity. Due to the improved aqueous compatibility, the emission spectra of MPS in fresh HeLa cell suspension was following collected and compared with the fluorescence spectra of MPS in organic solvents. It was found that the emission spectra from cell suspension and ethanol were quite similar, implying that the micro-environmental polarity of the organelle where MPS accumulated was very close to that of ethanol (Figure 1A inset). The fluorescence responses of MPS towards various common biologically relevant species were examined (Figure S2) and no noticeable change was observed.

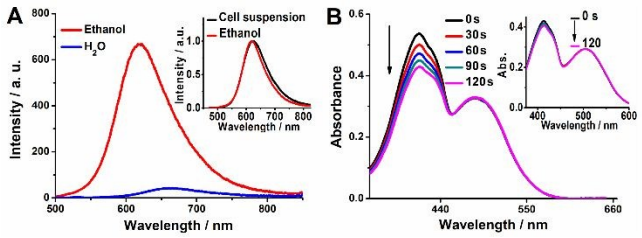

Figure 1. (A) Emission spectra of MPS (5 μM) in ethanol (red) and in water (blue) normalized to the absorbance at the excitation wavelength. Inset shows the normalized fluorescence spectra of MPS (5 μM) in HeLa cell suspension (black) and in ethanol (red). (B) Time dependent absorption of DPBF (20 μM) mixed with MPS (10 μM) in ethanol and 1:1 (v/v) ethanol-water mixture (inset) upon 532 nm laser diode irradiation with power density of 80 mW cm^{-2}.

The ROS generation efficacy of MPS and P1 at different environments was next examined using 1, 3-diphenylisobenzofuran (DPBF) as a singlet oxygen trap. As shown in Figure 1B and S3, the absorbances around 410nm significantly decreased upon exciting either of the two mixtures of DPBF with MPS and P1 in ethanol. The $^1O_2$ quantum yield was estimated to be 0.15 and 0.16, respectively. When the polarity of the solvents increased from pure ethanol to 1:1 (v/v) water and ethanol mixture, both of the $^1O_2$ producibility of MPS and P1 were highly suppressed and the $^1O_2$ quantum yield was dropped to be 0.02 and 0.03 respectively which indicated that the photosensitizing functions of the dibenzylideneacetone derivatives were environment-dependent even -activatable. The photostability of MPS and P1 were also examined by monitoring their fluorescence changes under the light irradiation (40 mW cm^{-2}) for different times. As shown in Figure S4, neglectable emission change of either MPS or P1 was observed after 150 s irradiation. These *in vitro* photophysical assays together exhibit MPS a potential as a photostable environment-dependent and -activatable photosensitizer for controllable cancer cell photoablation and self-bioimaging.

Before evaluating the photoablation efficacy towards cancer cells, the intracellular staining and localization of MPS and P1 were both determined in HeLa cells and A431 cells using confocal fluorescence microscopy in combination with a commercially available mitochondrial tracking dye, MitoTracker Green FM (Figure S5). Different from the low uptake efficiency as well as the aimless distribution of P1 nanoaggregates in cells, the bright red emission and high staining overlap between MPS and MitoTracker with a Pearson's correlation coefficients of over 0.95 demonstrated the selected accumulation of MPS on

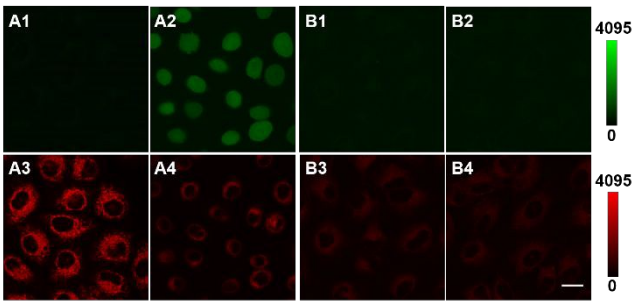

Figure 2. Images of MPS (A) and P1 (B) incubated HeLa cells co-stained with DCHF-DA in the absence (1 and 3) and presence (2 and 4) of white light LED irradiation (15 s, 40 mW cm^{-2}). Cell lines were first incubated with MPS (5 μM) or P1 (5 μM) for 30 min then subjected to irradiation for 15 s. After another 15 min incubation, all cells were stained with DCHF-DA (10 μM). (1-2) Green channel for DCF (EX: 488 nm, Em: 500-520 nm). (3-4) Red channel for MPS or P1 (EX: 488 nm, Em: 580-640 nm). The scale bar represents 20 μm for all the images.

mitochondria. The specific affinity of MPS towards mitochondria was further examined by an MMP disruption assay in which carbonyl cyanide m-chlorophenyl hydrazine (CCCP), a mitochondrial depolarizing reagent, was used. CCCP can induce MMP loss and mitochondria disruption then lose the affinity with lipophilic cations. After treated cells with CCCP, the bright emission of MPS almost faded (in Figure S6), illustrating that the mitochondria-targeting and -responsive property possessed by MPS is MMP-dependent. By combining the environment-sensitive emission property of MPS in Figure 1, it can be inferred that the MMP loss engenders MPS leak from mitochondria of low polarity to cytosol of high polarity accompanied with the fluorescence quenching, which verified the validity of MPS as a new indicator of mitochondria activity.

The intracellular versatilities of the two dibenzylideneacetone derivatives were next explored encouraged by their superior performances *in vitro*. we first measured the ROS producibilities of MPS and P1 in HeLa cells and A431 cells using 2',7'-dichlorodihydrofluorescin diacetate (DCHF-DA) as an indicator. DCHF-DA is non-fluorescent but can be oxidized by ROS to 2',7'-dichlorofluorescin (DCF), which emits strong green fluorescence. As shown in Figure 2 and S7, only cells that were treated with MPS followed by white light irradiation show the green DCF signal, which confirmed that MPS was able to generate ROS efficiently in cells upon light irradiation. The extremely low intracellular ROS productivity of P1 is possibly due to the poor membrane permeability as well as the intracellular aimless dispersion of P1 nanoaggregates. Subsequently, the cell apoptosis induced by MPS generated ROS was examined by staining cells with the Annexin V-FITC conjugate which possesses a special affinity with phosphatidylserine exposed on the plasma membrane surface of early apoptotic cells. As shown in Figure 3 and S8, both the two cell lines sheltered from white light showed only strong red fluorescence from MPS at mitochondria region but no green emission from cell membrane. After irradiation for 15 s, cell lines labelled by Annexin V-FITC presented characteristic green

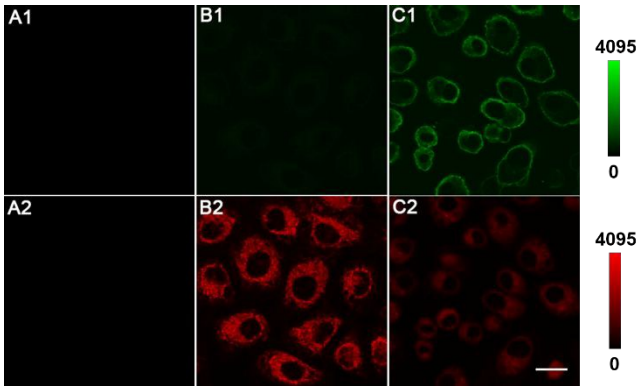

Figure 3. (A) Images of HeLa cells without MPS treatment in the presence of white light irradiation (15 s, 40 mW cm^{-2}), HeLa cells with MPS treatment (5 μM) in the absence (B) and presence (C) of white light irradiation (15 s, 40 mW cm^{-2}). Cell lines were first incubated with MPS (5 μM) for 30 min then subjected to irradiation for 15 s. After another 90 min incubation, all cells were stained with Annexin V-FITC. (A1-C1) Green channel for Annexin V-FITC (EX: 488 nm, EM: 500-520 nm); (A2-C2) Red channel for MPS (EX: 488 nm, EM: 580-640 nm); The scale bar represents 20 μm for all the images.

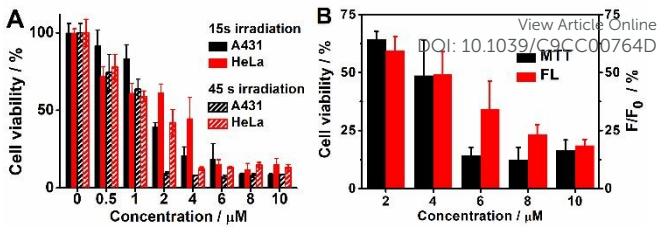

Figure 4. (A) Relative cell viability of cancer cells treated with various concentrations of MPS upon white light irradiation (40 mW cm^{-2}) for 15 and 45 s, respectively. (B) Comparison between MTT method and MPS fluorescence method (FL) for monitoring Hela cell viability during photodynamic treatment with MPS (EX: 488 nm, EM: 600 nm).

membrane staining, meaning cell apoptosis occurred, while the red fluorescence of MPS in mitochondria was synchronously decreased, showing the expectation of MPS to be a mitochondria-activatable photosensitizer and a synchronous tracer of the photoablation effect. The response of MPS to cell apoptosis was further validated by addition of exogenous ROS. MPS-incubated A431 cells were treated with 400 μM hydrogen peroxide (H_2O_2) to induce cell apoptosis and followed by subjected to Annexin V-FITC conjugate. The staining results were shown in Figure S9. The weakened red fluorescence emission on mitochondria accompanied by the bright green emission at the cell membrane region reconfirmed that MPS could be as a turn-off indicator for ROS-induced cell apoptosis. Taken together, these results validate that MPS can not only be a mitochondria-responsive and -activatable photosensitizer to controllably release ROS inducing cell apoptosis but also a built-in tracer for evaluation of the photoablation effect via its fluorescence signal changes.

The cytotoxicity of MPS for cancer cells was more evaluated by using 3-(4,5-dimethyl-2-thiazolyl)-2,5-diphenyl-2-H-tetrazolium bromide (MTT) assay. As in Figure S10, MPS showed low toxicity to HeLa cells and A431 cells in dark, revealing their relatively inert property without photoexcitation. Upon white light irradiation, significant cytotoxicity was soon caused by only treated the both cell lines with 2 μM of MPS, and prolonging the time of irradiation increased the photocytotoxicity (Figure 4A). In contrast, only moderate phototoxicity of P1 aggregates to the two cell lines were observed even at high concentrations (Figure S11) which was consistent with the results of DCHF-DA assay. The prompt and high photocytotoxicity of MPS is rationalized by the precise mitochondria-targeting, efficient ROS generation and consequent induced apoptosis. The half-maximal inhibitory concentration (IC_{50}) of MPS upon light irradiation at 0.6 J cm^{-2} (15 s irradiation) to HeLa cells and A431 cells was determined to be 3.2 and 1.9 μM, respectively, which confirmed that MPS is an efficient PS for photodynamic ablation of cancer cells. Furthermore, the fluorescence change (F/F_0) of MPS-incubated HeLa cells before and after irradiation was examined. The value was well related with the cell viability evaluated by MTT assays in Figure 4B which reconfirmed that MPS could traceably report the cell apoptosis induced by itself generated ROS.

In conclusion, we have rationally designed and synthesized a couple of dibenzylideneacetone derivatives P1 and MPS, in which MPS presents environment-sensitive on-off fluorescence and activatable photosensitizing abilities. Under the guidance of pyridinium unit, MPS mainly accumulates on mitochondrial

components with bright red emission and silent photoablation. Upon light irradiation, copious ROS are generated from mitochondria which causes MMP loss and cell apoptosis. Then the red emission on mitochondrial components turns off and the ROS generation is ceased due to the MMP disruption induced MPS leakage from mitochondria to cytosol. The integrated functionalities of target-controlled photoablation and self-efficacy traceability offer MPS a new opportunity for visualized and hazard-free cancer PDT with synchronous evaluation of the therapeutic responses.

This work was supported by the National Natural Science Foundation of China (21233011 , 21205122) and Youth Innovation Promotion Association (2017032) of Chinese Academy of Sciences.

Conflicts of interest

There are no conflicts to declare.

Notes and references

1. T. J. Dougherty, C. J. Gomer, B. W. Henderson, G. Jori, D. Kessel, M. Korbelik, J. Moan and Q. Peng, *JNCI: Journal of the National Cancer Institute*, 1998, **90**, 889-905.
2. I. J. MACDONALD and T. J. DOUGHERTY, *Journal of Porphyrins and Phthalocyanines*, 2001, **05**, 105-129.
3. R. Bonnett and G. Marťınez, *Tetrahedron*, 2001, **57**, 9513-9547.
4. E. S. Nyman and P. H. Hynninen, *Journal of Photochemistry and Photobiology B: Biology*, 2004, **73**, 1-28.
5. C. W. Brian and S. P. Michael, *Physics in Medicine & Biology*, 2008, **53**, R61.
6. B. C. Wilson and M. S. Patterson, *Phys Med Biol*, 2008, **53**, R61-R109.
7. J. Tian, L. Ding, H. J. Xu, Z. Shen, H. Ju, L. Jia, L. Bao and J. S. Yu, *Journal of the American Chemical Society*, 2013, **135**, 18850-18858.
8. J. F. Lovell, T. W. B. Liu, J. Chen and G. Zheng, *Chemical Reviews*, 2010, **110**, 2839-2857.
9. A. P. Castano, P. Mroz and M. R. Hamblin, *Nat Rev Cancer*, 2006, **6**, 535-545.
10. I. Noh, D. Lee, H. Kim, C. U. Jeong, Y. Lee, J. O. Ahn, H. Hyun, J. H. Park and Y. C. Kim, *Adv Sci*, 2018, **5**.
11. G. A. M. S. van Dongen, G. W. M. Visser and M. B. Vrouenraets, *Advanced Drug Delivery Reviews*, 2004, **56**, 31-52.
12. C. L. Conway, I. Walker, A. Bell, D. J. H. Roberts, S. B. Brown and D. I. Vernon, *Photochemical & Photobiological Sciences*, 2008, **7**, 290-298.
13. Y. Yuan, G. Feng, W. Qin, B. Z. Tang and B. Liu, *Chemical communications*, 2014, **50**, 8757-8760.
14. Y. Yuan, C.-J. Zhang, M. Gao, R. Zhang, B. Z. Tang and B. Liu, *Angewandte Chemie International Edition*, 2015, **54**, 1780-1786.
15. M. Famulok, J. S. Hartig and G. Mayer, *Chemical Reviews*, 2007, **107**, 3715-3743.
16. G. Mayer, *Angewandte Chemie International Edition*, 2009, **48**, 2672-2689.
17. M. Zhang, Z. Zhang, D. Blessington, H. Li, T. M. Busch, V. Madrak, J. Miles, B. Chance, J. D. Glickson and G. Zheng, *Bioconjugate Chemistry*, 2003, **14**, 709-714.
18. W. Piao, K. Hanaoka, T. Fujisawa, S. Takeuchi, T. Komatsu, T. Ueno, T. Terai, T. Tahara, T. Nagano and Y. Urano, *Journal of the American Chemical Society*, 2017, **139**, 13713-13719.
19. J. Chen, K. Stefflova, M. J. Niedre, B. C. Wilson, B. Chance, J. D. Glickson and G. Zheng, *Journal of the American Chemical Society*, 2004, **126**, 11450-11451.
20. K. Stefflova, J. Chen, D. Marotta, H. Li and G. Zheng, *Journal of Medicinal Chemistry*, 2006, **49**, 3850-3856.
21. M. Chiba, Y. Ichikawa, M. Kamiya, T. Komatsu, T. Ueno, K. Hanaoka, T. Nagano, N. Lange and Y. Urano, *Angewandte Chemie International Edition*, 2017, **56**, 10418-10422.
22. T. Yogo, Y. Urano, A. Mizushima, H. Sunahara, T. Inoue, K. Hirose, M. Iino, K. Kikuchi and T. Nagano, *Proceedings of the National Academy of Sciences*, 2008, **105**, 28-32.
23. S. O. McDonnell, M. J. Hall, L. T. Allen, A. Byrne, W. M. Gallagher and D. F. O'Shea, *Journal of the American Chemical Society*, 2005, **127**, 16360-16361.
24. T. Tørring, R. Toftegaard, J. Arnbjerg, P. R. Ogilby and K. V. Gothelf, *Angewandte Chemie International Edition*, 2010, **49**, 7923-7925.
25. Y. Yuan, R. T. Kwok, B. Z. Tang and B. Liu, *Small*, 2015, **11**, 4682-4690.
26. Y. Yuan, C.-J. Zhang, S. Xu and B. Liu, *Chemical Science*, 2016, **7**, 1862-1866.
27. Y. Yuan, C.-J. Zhang, R. T. K. Kwok, S. Xu, R. Zhang, J. Wu, B. Z. Tang and B. Liu, *Advanced Functional Materials*, 2015, **25**, 6586-6595.
28. L. Galluzzi, N. Joza, E. Tasdemir, M. C. Maiuri, M. Hengartner, J. M. Abrams, N. Tavernarakis, J. Penninger, F. Madeo and G. Kroemer, *Cell Death And Differentiation*, 2008, **15**, 1113.
29. G. Kroemer, L. Galluzzi and C. Brenner, *Physiological Reviews*, 2007, **87**, 99-163.
30. H. S. Jung, J. H. Lee, K. Kim, S. Koo, P. Verwilst, J. L. Sessler, C. Kang and J. S. Kim, *Journal of the American Chemical Society*, 2017, **139**, 9972-9978.
31. S. Chakrabortty, B. K. Agrawalla, A. Stumper, N. M. Vegi, S. Fischer, C. Reichardt, M. Kogler, B. Dietzek, M. Feuring-Buske, C. Buske, S. Rau and T. Weil, *Journal of the American Chemical Society*, 2017, **139**, 2512-2519.
32. H. Wang, Z. Feng, Y. Wang, R. Zhou, Z. Yang and B. Xu, *Journal of the American Chemical Society*, 2016, **138**, 16046-16055.
33. G.-Y. Pan, H.-R. Jia, Y.-X. Zhu, R.-H. Wang, F.-G. Wu and Z. Chen, *ACS Biomaterials Science & Engineering*, 2017, **3**, 3596-3606.
34. S. Fulda, L. Galluzzi and G. Kroemer, *Nature Reviews Drug Discovery*, 2010, **9**, 447.
35. L. X. Cao, Z. S. Zhao, T. Zhang, X. D. Guo, S. Q. Wang, S. Y. Li, Y. Li and G. Q. Yang, *Chem Commun*, 2015, **51**, 17324-17327.
36. H. J. Kwon, D. Kim, K. Seo, Y. G. Kim, S. I. Han, T. Kang, M. Soh and T. Hyeon, *Angewandte Chemie International Edition*, 2018, **57**, 9408-9412.
37. C. L. Yang, R. Hu, Q. Li, S. Li, J. F. Xiang, X. D. Guo, S. Q. Wang, Y. Zeng, Y. Li and G. Q. Yang, Acs Omega, 2018, 3, 10487-10492.
38. N. J. Turro, V. Ramamurthy and J. C. Scaiano, *Photochemistry and Photobiology*, 2012, **88**, 1033-1033.
39. J. Rafael and D. Nicholls, *FEBS letters*, 1984, **170**, 181-185.

View Article Online
DOI: 10.1039/C9CC00764D

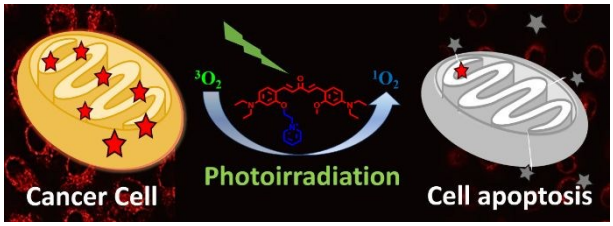

A mitochondria-responsive and -activatable photosensitizer MPS, with a built-in tracer for cancer cell photoablation was constructed.